

Topological parafermion corner states in clock-symmetric non-Hermitian second-order topological insulator

Motohiko Ezawa

Department of Applied Physics, University of Tokyo, Hongo 7-3-1, 113-8656, Japan

Parafermions are a natural generalization of Majorana fermions. We consider a breathing Kagome lattice with complex hoppings by imposing \mathbb{Z}_3 clock symmetry in the complex energy plane. It is a non-Hermitian generalization of the second-order topological insulator characterized by the emergence of topological corner states. We demonstrate that the topological corner states are parafermions in the present \mathbb{Z}_3 clock-symmetric model. It is also shown that the model is realized in electric circuits properly designed, where the parafermion corner states are observed by impedance resonance. We also construct \mathbb{Z}_4 and \mathbb{Z}_6 parafermions on breathing square and honeycomb lattices, respectively.

I. INTRODUCTION

Topological quantum computation is a fault-tolerant quantum computation¹⁻⁷. Majorana fermions provide us with a most studied platform of topological quantum computation⁸⁻¹³. The Majorana operator γ satisfies $\gamma^2 = 1$. They are realized as topological boundary states of topological superconductors¹⁴⁻¹⁹ and Kitaev spin liquids^{3,20}. However, it is impossible to perform universal quantum computation only by the braiding of Majorana fermions since they can reproduce only a part of Clifford gates²¹.

Parafermions are straightforward generalization of Majorana fermions²²⁻²⁶, where the parafermion operator γ satisfies $\gamma^d = 1$ for $d \geq 3$. Braiding of parafermions with $d = 3$ are known to reproduce all the Clifford gates²⁷ although universal quantum computation is not yet possible. In this sense, parafermions are more powerful than Majorana fermions in the context of quantum computation. Parafermions are realized in clock-spin models^{23,28}, fractional quantum Hall effects^{29,30}, fractional topological superconductors³¹ and twisted bilayer graphene³². Among them, the \mathbb{Z}_d clock-spin model²⁸ is non-Hermitian and its energy spectrum is \mathbb{Z}_d symmetric in the complex plane. It is an interesting problem if they also emerge as topological boundary states in certain lattice structures just as Majorana fermions do.

Higher-order topological insulators and superconductors are generalization of topological insulators and superconductors³³⁻⁴⁶. They are prominent by the emergence of zero-energy corner states instead of gapless edge states. These zero-energy corner states are topologically protected. A typical example is given by the breathing Kagome lattice⁴², where three topological corner states emerge. There are some generalization to non-Hermitian higher-order topological insulators⁴⁷⁻⁵⁰.

In this paper, generalizing the breathing Kagome second-order topological insulator model by imposing \mathbb{Z}_3 clock symmetry, we propose a new type of non-Hermitian higher-order topological insulator, where the topological corner states are parafermions. This model is non-Hermitian, where the energy spectrum is \mathbb{Z}_3 symmetric in the complex energy plane as in the case of the \mathbb{Z}_3 clock-spin model. We demonstrate how to implement the present model of parafermions in an electric circuit. We also construct \mathbb{Z}_4 and \mathbb{Z}_6 parafermions as topolog-

ical corner states on breathing square and honeycomb lattices.

II. MAJORANA FERMION AND PARA-FERMION

Majorana fermion operators γ_i satisfy the relations

$$(\gamma_j)^2 = 1, \quad \gamma_j \gamma_k = -\gamma_k \gamma_j. \quad (1)$$

Majorana fermions are realized as zero-energy states of a topological superconductor, where particle-hole symmetry (PHS) preserves. It is understood as follows. The PHS operator Ξ acts as $\Xi^{-1} H \Xi = -H$ with the eigen equation $H |\psi\rangle = E |\psi\rangle$. If a particle has an energy E , its antiparticle has the energy $-E$ in the presence of PHS. Namely, the wave functions always appear in a particle-hole pair with a pair of energies $(E, -E)$. If the states satisfy the relation $E = -E$, the particle is identical to its antiparticle, and a pair of Majorana fermions emerge. Hence, the zero-energy ($E = 0$) states respecting PHS are Majorana states.

Parafermions are natural generalization of Majorana fermions. \mathbb{Z}_d parafermions are defined through the relations

$$(\gamma_j)^d = 1, \quad \gamma_j \gamma_k = \omega \gamma_k \gamma_j, \quad (2)$$

where $\omega = e^{2\pi i/d}$. The minimal model consists of two elements γ_1 and γ_2 .

III. \mathbb{Z}_3 PARA-FERMION

We start with a minimal model by setting $d = 3$ in Eq.(2). \mathbb{Z}_3 parafermions are represented by the shift operator^{23,24,51}

$$\gamma_1 \equiv \tau = \begin{pmatrix} 0 & 0 & 1 \\ 1 & 0 & 0 \\ 0 & 1 & 0 \end{pmatrix}, \quad (3)$$

and the clock operator^{23,24,51}

$$\gamma_2 \equiv \sigma = \text{diag.} (1, \omega, \omega^2), \quad (4)$$

where $\omega = e^{2\pi i/3}$. Here, τ and σ satisfy the \mathbb{Z}_3 parafermion relations,

$$\tau^3 = \sigma^3 = 1, \quad \sigma \tau = \omega \tau \sigma. \quad (5)$$

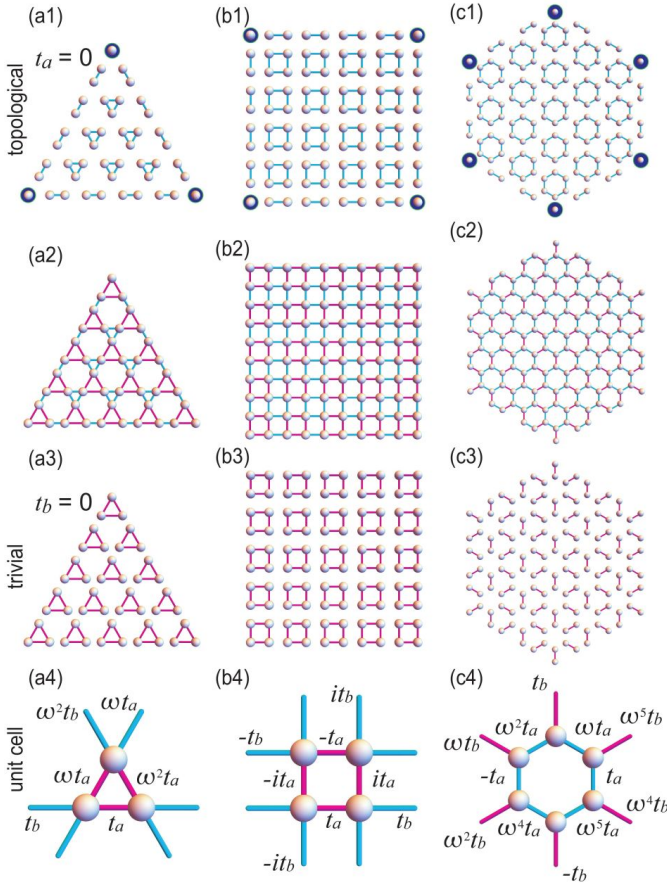


FIG. 1: (a) Breathing Kagome lattice, (b) breathing square lattice and (c) breathing honeycomb lattice. The hopping parameters are $t_a = 0$ for (a1)~(c1), $t_a t_b \neq 0$ for (a2)~(c2), and $t_b = 0$ for (a3)~(c3). There emerge three, four and six parafermion corner states in the topological phase. When $t_a = 0$, they are isolated as marked by blue disks in (a1), (b1) and (c1), respectively. The unit cells are given in (a4), (b4) and (c4) with the hopping parameters indicated.

In the \mathbb{Z}_3 clock-symmetric model, the energy spectrum is composed of triplets²⁸ $E_n^{(0,1,2)}$, $n = 0, 1, 2, \dots$,

$$E_n^{(0,1,2)} = \varepsilon_n, \quad \omega \varepsilon_n, \quad \omega^2 \varepsilon_n, \quad (6)$$

satisfying $\varepsilon_n + \omega \varepsilon_n + \omega^2 \varepsilon_n = 0$. The system is necessarily non-Hermitian because the eigen energies are complex except for zero-energy states.

A. Zero-energy parafermion states

It follows from Eq.(6) that only the zero-energy states form a set of degenerate states respecting \mathbb{Z}_3 clock symmetry. They are \mathbb{Z}_3 parafermion states. We denote them as $|\psi_0\rangle, |\psi_1\rangle$ and

$|\psi_2\rangle$. They are characterized by the properties

$$\tau |\psi_0\rangle = |\psi_1\rangle, \quad \tau |\psi_1\rangle = |\psi_2\rangle, \quad \tau |\psi_2\rangle = |\psi_0\rangle, \quad (7)$$

$$\sigma |\psi_0\rangle = |\psi_0\rangle, \quad \sigma |\psi_1\rangle = \omega |\psi_1\rangle, \quad \sigma |\psi_2\rangle = \omega^2 |\psi_2\rangle, \quad (8)$$

from which the matrix representations (3) and (4) follow. Then, the \mathbb{Z}_3 parafermion relations (5) are verified. Namely, it is necessary and sufficient to examine Eqs.(7) and (8) for a triplet set of zero-energy states in order to show that they are \mathbb{Z}_3 parafermions.

B. Breathing Kagome lattice

We propose a model possessing parafermions on the breathing Kagome lattice. The bulk Hamiltonian is given by

$$H = \begin{pmatrix} 0 & h_{12} & \omega h_{13} \\ h_{12}^* & 0 & \omega^2 h_{23} \\ \omega h_{13}^* & \omega^2 h_{23}^* & 0 \end{pmatrix}, \quad (9)$$

with

$$h_{12} = t_a + t_b e^{ik_x}, \quad (10)$$

$$h_{23} = t_a + t_b e^{-i(k_x/2 + \sqrt{3}k_y/2)}, \quad (11)$$

$$h_{13} = t_a + t_b e^{-i(k_x/2 - \sqrt{3}k_y/2)}, \quad (12)$$

where we have introduced two hopping parameters t_a and t_b , corresponding to the magenta link and the cyan link along the horizontal axis in Fig.1(a4). The hopping parameters along the other two triangle sides are given by ωt_a and $\omega^2 t_a$ for a magenta triangle, and ωt_b and $\omega^2 t_b$ for a cyan triangle. This model is non-Hermitian due to the presence of ω .

A comment is in order with respect to the breathing Kagome model. It is a typical model for the conventional second-order topological insulator⁴², where the factor ω is absent and it is Hermitian. The present generalization of the breathing Kagome lattice model provides us with a new type of non-Hermitian second-order topological insulators.

C. Clock symmetry

The Hamiltonian (9) has \mathbb{Z}_3 clock symmetry²³,

$$\tau H(\mathbf{k}) \tau^\dagger = \omega H(R\mathbf{k}), \quad (13)$$

where R rotates the momentum by 120 degrees as

$$R(k_x, 0) = \left(-\frac{k_x}{2}, \frac{\sqrt{3}k_y}{2}\right), \quad (14)$$

$$R\left(-\frac{k_x}{2}, \frac{\sqrt{3}k_y}{2}\right) = \left(-\frac{k_x}{2}, -\frac{\sqrt{3}k_y}{2}\right), \quad (15)$$

$$R\left(-\frac{k_x}{2}, -\frac{\sqrt{3}k_y}{2}\right) = (k_x, 0), \quad (16)$$

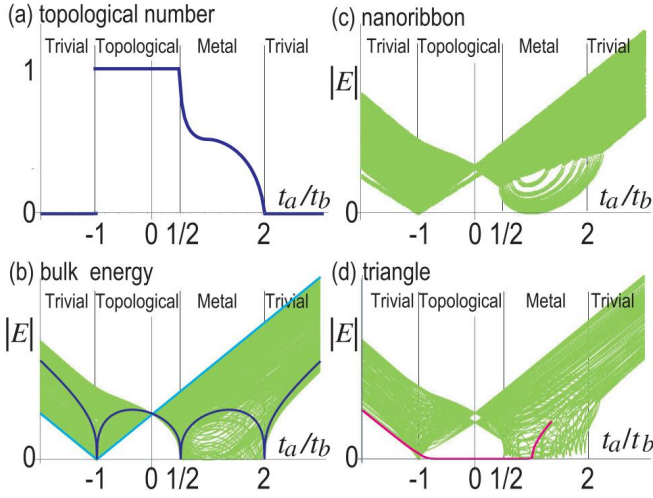


FIG. 2: (a) Topological number (21) as a function of t_a/t_b . It is quantized in the insulators. (b)~(c) Energy spectrum as a function of t_a/t_b for (b) the bulk, (c) a nanoribbon with width 64, and (d) a triangle with size 20. In (b), the blue curves represent the bulk energy (20) at the K and K' points, and the cyan lines represent the bulk energy (19) at the Γ point, which are analytically obtained. In the topological phase, gapless edge states are absent in nanoribbon geometry as in (c), but zero-energy corner states emerge in triangle geometry as indicated by the magenta flat-line segment in (d). The segment slightly deviates from the region $(-1, 1/2)$ due to the finite size effect.

making the energy spectrum have \mathbb{Z}_3 symmetry in the complex plane as in Eq.(6). In addition, there is an anti-unitary symmetry

$$KH(\mathbf{k})K = H^*(\mathbf{k}), \quad (17)$$

where K implies complex conjugate. It leads to reflection symmetry between E and E^* . As a result, the energy spectrum has C_{3v} symmetry in the complex plane, which consists of the three-fold rotational symmetry and three reflection symmetries.

The system also has a generalized chiral symmetry for a three-band model⁵²,

$$\begin{aligned} \sigma H \sigma^{-1} &= H_1, & \sigma H_1 \sigma^{-1} &= H_2, \\ H + H_1 + H_2 &= 0. \end{aligned} \quad (18)$$

We show the bulk energy spectrum in Fig.3(a) and Fig.4(a), where C_{3v} symmetry is manifest for all parameters.

D. Phase diagram

The notion of insulator and metal is generalized to the non-Hermitian Hamiltonian in two ways. On is a point-gap insulator^{53,54}, where $|E|$ has a gap. The other is a line-gap insulator^{53,54}, where $\text{Re}[E]$ or $\text{Im}[E]$ has a gap. In our model, we adopt the definition of the point-gap insulator due to \mathbb{Z}_3

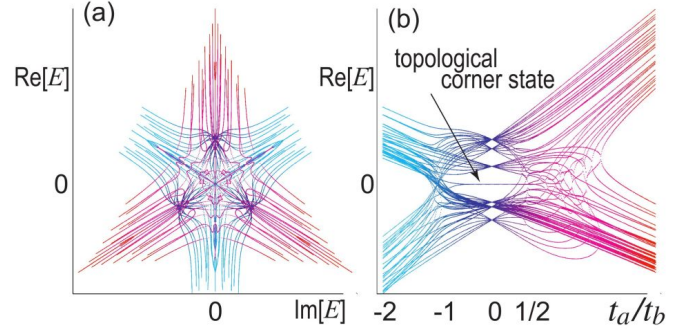


FIG. 3: Energy spectrum of a triangle, where (a) the vertical axis is $\text{Re}[E]$ and the horizontal axis is $\text{Im}[E]$, while (b) the horizontal axis is t_a/t_b . Color indicates the value of t_a/t_b , where the color pallet is the same as in (b). C_{3v} symmetry in the complex energy plane is manifest in (a). The emergence of zero-energy corner states is clear in (b). We have used a triangle with size 6.

symmetry. We are able to determine the energy spectrum analytically at the $\Gamma = (0, 0)$ point as

$$E(0, 0) = (t_a + t_b), \quad \omega(t_a + t_b), \quad \omega^2(t_a + t_b), \quad (19)$$

and at the $K = (4\pi/3, 0)$ and $K' = (-4\pi/3, 0)$ points as

$$E^3(\pm 4\pi/3, 0) = (t_a + t_b)(t_a - 2t_b)(2t_a - t_b). \quad (20)$$

The point gap closes at the K and K' points for $t_a/t_b = 1/2$, $t_a/t_b = 2$, and at the K , K' and Γ points for $t_a/t_b = -1$, as in Fig.2(b). This is also confirmed numerically by calculating the band spectrum as in Fig.2(b).

E. Topological number

The topological number is given by the Berry phase defined by

$$Q \equiv \frac{1}{2\pi i} \int_0^{2\pi} \langle \psi_0(k_x, 0) | \partial_{k_x} | \psi_0(k_x, 0) \rangle dk_x, \quad (21)$$

where ψ_0 is the eigen function of the Hamiltonian (9) for the bulk, whose eigen energy is real along the k_x axis (i.e., $k_y = 0$). We calculate it numerically, whose results are shown in Fig.2(a). We find $Q = 1$ for $-1 < t_a/t_b < 1/2$, and $Q = 0$ for $t_a/t_b < -1$ and $t_a/t_b > 2$, while it continuously changes from 1 to 0 for $1/2 < t_a/t_b < 2$. In fact, Q is quantized in the insulator phases.

F. Edge states

We calculate the energy spectrum in a nanoribbon numerically. Edge states are observed in Fig.4(a2)~(h2), where the complex energy spectrum is shown for various momentum k specified by color. Three-fold symmetry is slightly broken in nanoribbon geometry. It is due to the finite size effect of a nanoribbon.

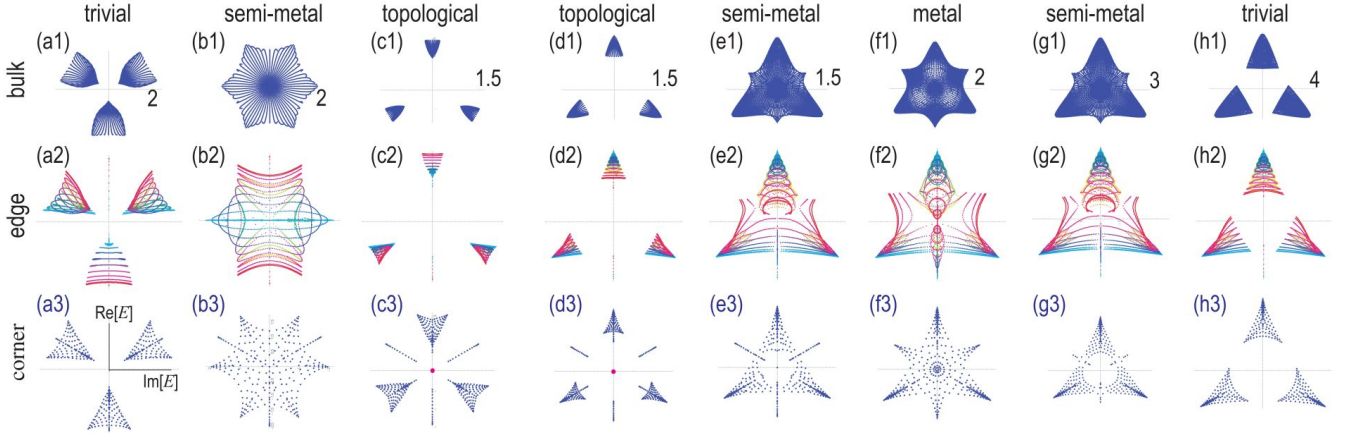


FIG. 4: Complex energy spectrum (a1)~(h1) for the bulk, (a2)~(h2) for a nanoribbon and (a3)~(h3) for a triangle, where the hopping parameters are (a1)~(a3) $t_a = -1.5t_b$, (b1)~(b3) $t_a = -t_b$, (c1)~(c3) $t_a = -0.25t_b$, (d1)~(d3) $t_a = 0.25t_b$, (e1)~(e3) $t_a = 0.5t_b$, (f1)~(f3) $t_a = 1.25t_b$, (g1)~(g3) $t_a = 2t_b$ and (h1)~(h3) $t_a = 2.5t_b$. The horizontal axis is $\text{Im}[E]$ and the vertical axis is $\text{Re}[E]$. The numerical value on the horizontal axis in (a1)~(h1) is the energy in unit of t_b . Color indicates the momentum of along the nanoribbon direction, where red color indicates $k = \pi$ and blue color indicates $k = 0$ in a nanoribbon. We have used a nanoribbon with width 128 for (a2)~(h2), and a triangle with size 16 for (a3)~(h3). The magenta dots in (c3) and (d3) represent the topological corner states.

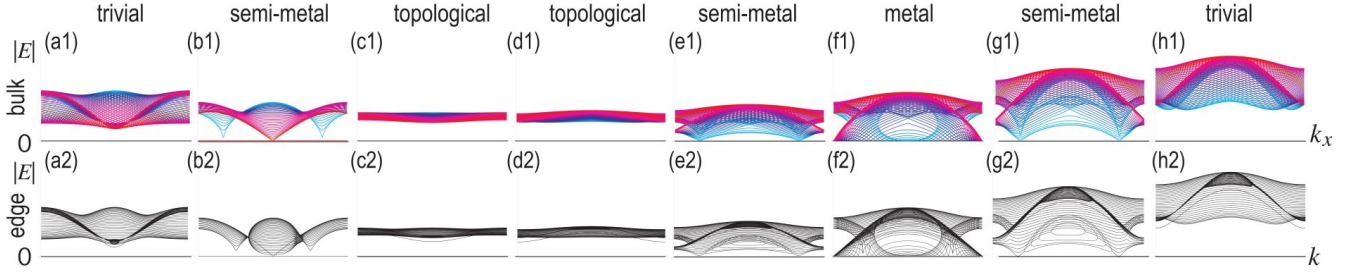


FIG. 5: (a1)~(h1) Bulk band structure, where the horizontal axis is k_x . Color in the spectrum indicates k_y , where red color indicates $k_y = 0$ while cyan color indicates $k_y = 2\pi/\sqrt{3}$. (a2)~(h2) Band structure of a nanoribbon, where the horizontal axis is k . The vertical axis is $|E|$. The values of t_a and t_b are the same as in Fig.4. It is notable that there are no gapless edge states in the topological phase.

We present the band structure of a nanoribbon in Fig.5(a2)~(h2), where we observe the absence of gapless edge states in the topological phase.

G. Corner states

We calculate the energy spectrum in triangle geometry numerically. C_{3v} symmetry is manifest as shown in Fig.3(a) and in Fig.4(a3)~(h3). It is because the triangle respects \mathbb{Z}_3 clock symmetry. We find zero-energy states in the region $-1 < t_a/t_b < 1/2$, as indicated by a magenta line in Fig.2(d). We also show the energy spectrum as a function of t_a/t_b in Fig.3(b), where the emergence of the zero-energy states is manifest in the topological phase.

Consequently, the present model is a second-order topological insulator in the region $-1 < t_a/t_b < 1/2$, being characterized by the emergence of topological corner states.

It is possible to obtain explicitly the wave functions of the three corner states by numerical calculation. We have numerically confirmed that they satisfy the relations (7) and (8).

Therefore, they are \mathbb{Z}_3 parafermions.

H. Electric-circuit implementation

Electric circuits are governed by the Kirchhoff current law. By making the Fourier transformation with respect to time, the Kirchhoff current law is expressed as

$$I_a(\omega) = \sum_b J_{ab}(\omega) V_b(\omega), \quad (22)$$

where I_a is the current between node a and the ground, while V_b is the voltage at node b . The matrix $J_{ab}(\omega)$ is called the circuit Laplacian. Once the circuit Laplacian is given, we can uniquely setup the corresponding electric circuit. By equating it with the Hamiltonian H as^{55,56}

$$J_{ab}(\omega) = i\omega H_{ab}(\omega), \quad (23)$$

it is possible to simulate various topological phases of the Hamiltonian by electric circuits^{46,48,49,55-63}. The relations be-

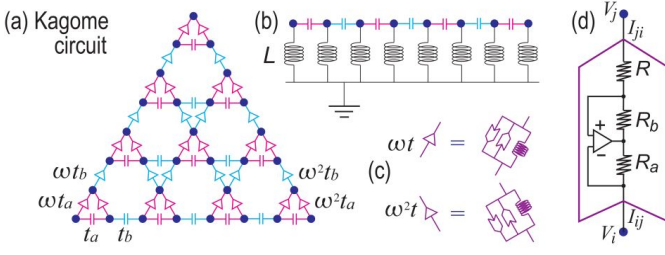


FIG. 6: (a) Illustration of the breathing Kagome circuit corresponding to Fig.1(a). (b) Each node is grounded by an inductor. (c) Complex hoppings $\propto e^{\pm 2\pi i/3}$ are realized by a parallel connection of an inductor and an operational amplifier. We show a triangle with size 4.

tween the parameters in the Hamiltonian and in the electric circuit are determined by this formula.

The circuit Laplacian is constructed as follows. To simulate the positive and negative hoppings in the Hamiltonian, we replace them with the capacitance $i\omega C$ and the inductance $1/i\omega L$, respectively. We note that $\sin k = (e^{ik} - e^{-ik})/2i$ represents an imaginary hopping in the tight-bind model. The imaginary hopping is realized by an operational amplifier⁶².

We thus make the following replacements with respect to hoppings in the Hamiltonian to derive the circuit Laplacian: (i) $+X \rightarrow i\omega C_X$ for $X = t_a$ and t_b , where C_X represents the capacitance whose value is X [pF]. (ii) $-X \rightarrow 1/i\omega L_X$ for $X = t_a/2$ and $t_b/2$, where L_X represents the inductance whose value is X [μ H].

We explicitly study the breathing Kagome lattice described by (9), where the electric circuit is given by Fig.6(a). The Hamiltonian (9) is decomposed into

$$H = H_1 + H_2, \quad (24)$$

with

$$H_1 = \begin{pmatrix} 0 & h_{12} & -\frac{1}{2}h_{13} \\ h_{12}^* & 0 & \omega^2 h_{23} \\ -\frac{1}{2}h_{13}^* & \omega^2 h_{23}^* & 0 \end{pmatrix} \quad (25)$$

and

$$H_2 = \frac{\sqrt{3}}{2} \begin{pmatrix} 0 & 0 & ih_{13} \\ 0 & 0 & -ih_{23} \\ ih_{13}^* & -ih_{23}^* & 0 \end{pmatrix}, \quad (26)$$

where H_1 is Hermitian ($H_1^\dagger = H_1$), and H_2 is anti-Hermitian ($H_2^\dagger = -H_2$). It is necessary to construct imaginary hopping Hamiltonians

$$\frac{\sqrt{3}}{2}t_a \begin{pmatrix} 0 & 0 & i \\ 0 & 0 & 0 \\ i & 0 & 0 \end{pmatrix}, \quad (27)$$

and

$$\frac{\sqrt{3}}{2}t_a \begin{pmatrix} 0 & 0 & 0 \\ 0 & 0 & -i \\ 0 & -i & 0 \end{pmatrix} \quad (28)$$

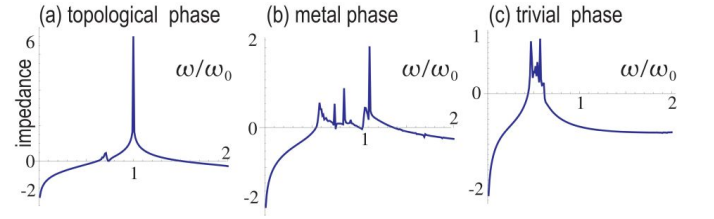


FIG. 7: Impedance as a function of ω . The vertical axis is $\log_{10} Z$ and the horizontal axis is ω/ω_0 . (a) topological phase with $t_a/t_b = 0.25$, (b) metallic phase with $t_a/t_b = 1$ and (c) trivial phase with $t_a/t_b = 2.5$. A prominent peak is found in the topological phase.

for the magenta lines in Fig.6(a). They are constructed by using operational amplifiers and resistors.

We review a negative impedance converter with current inversion based on an operational amplifier with resistors⁶². The voltage-current relation for the operational amplifier circuit is given by⁶²

$$\begin{pmatrix} I_1 \\ I_2 \end{pmatrix} = \frac{1}{R} \begin{pmatrix} -\nu & \nu \\ -1 & 1 \end{pmatrix} \begin{pmatrix} V_1 \\ V_2 \end{pmatrix}, \quad (29)$$

with $\nu = R_b/R_a$, where R , R_a and R_b are the resistances in an operational amplifier: See Fig.6(d). We note that the resistors in the operational amplifier circuit are tuned to be $\nu = 1$ in the literature⁶² so that the system becomes Hermitian, where the corresponding Hamiltonian represents a spin-orbit interaction.

In this paper, we use two negative impedance converters parallelly connected with the opposite direction as in Fig.6(c). The circuit Laplacian due to these two converters is given by

$$\frac{1}{R} \left[\begin{pmatrix} -\nu & \nu \\ -1 & 1 \end{pmatrix} + \begin{pmatrix} 1 & -1 \\ \nu & -\nu \end{pmatrix} \right] = \frac{1}{R} \begin{pmatrix} 1-\nu & \nu-1 \\ \nu-1 & 1-\nu \end{pmatrix}. \quad (30)$$

It corresponds to the Hamiltonian

$$H = \frac{1}{i\omega R} \begin{pmatrix} 1-\nu & \nu-1 \\ \nu-1 & 1-\nu \end{pmatrix}. \quad (31)$$

It is embedded in the 3×3 matrix as

$$H = \frac{1}{i\omega R} \begin{pmatrix} 1-\nu & 0 & \nu-1 \\ 0 & 0 & 0 \\ \nu-1 & 0 & 1-\nu \end{pmatrix}, \quad (32)$$

where we have set

$$\frac{\sqrt{3}}{2}t_a = \frac{1-\nu}{\omega R} \quad (33)$$

with $\nu < 1$, and

$$H = \frac{1}{i\omega R} \begin{pmatrix} 0 & 0 & 0 \\ 0 & 1-\nu & \nu-1 \\ 0 & \nu-1 & 1-\nu \end{pmatrix}, \quad (34)$$

where we have set

$$\frac{\sqrt{3}}{2}t_a = \frac{\nu-1}{\omega R} \quad (35)$$

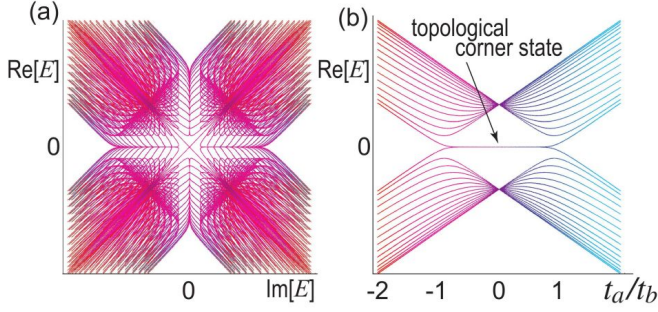


FIG. 8: Energy spectrum of a square, where (a) the vertical axis is $\text{Re}[E]$ and the horizontal axis is $\text{Im}[E]$, while (b) the horizontal axis is t_a/t_b . Color indicates the value of t_a/t_b , where the color pallet is the same as in (b). C_{4v} symmetry in the complex energy plane is manifest in (a). The emergence of zero-energy corner states is clear in (b).

with $\nu > 1$. These matrices are different from Eqs.(27) and (28) by the diagonal terms. They are cancelled by adding a resistor (for $\nu > 1$) or an operational amplifier (for $\nu < 1$) with the amount of

$$\frac{1 - \nu}{i\omega R} \quad (36)$$

between a lattice site and the ground.

I. Impedance resonance

The zero-energy parafermion corner states are well observed by impedance resonance, which is defined⁵⁷ by

$$Z_{ab} = V_a/I_b = G_{ab} \quad (37)$$

where $G = J^{-1}$ is the Green function. It diverges at the frequency where the admittance is zero ($J = 0$). Taking the nodes a and b at two corners, we show the impedance in topological, metallic and trivial phases in Figs.7(a)~(c), respectively. A strong impedance peak is observed at the critical frequency $\omega_0 \equiv 1/\sqrt{LC}$ only in the topological phase. It signals the emergence of zero-energy parafermion corner states.

IV. \mathbb{Z}_4 PARA-FERMION

We proceed to a model with $d = 4$. \mathbb{Z}_4 parafermions are represented by the shift operator^{23,24,51}

$$\gamma_1 \equiv \tau = \begin{pmatrix} 0 & 0 & 0 & 1 \\ 1 & 0 & 0 & 0 \\ 0 & 1 & 0 & 0 \\ 0 & 0 & 1 & 0 \end{pmatrix}, \quad (38)$$

and the clock operator^{23,24,51}

$$\gamma_2 \equiv \sigma = \text{diag.} (1, i, -1, -i). \quad (39)$$

Here, τ and σ satisfy the \mathbb{Z}_4 parafermion relations,

$$\tau^4 = \sigma^4 = 1, \quad \tau\sigma = \omega\sigma\tau. \quad (40)$$

In the \mathbb{Z}_4 clock-symmetric model, the energy spectrum is composed of quartets $E_n^{(0,1,2,3)}$, $n = 0, 1, 2, \dots$,

$$E_n^{(0,1,2,3)} = \varepsilon_n, \quad i\varepsilon_n, \quad -\varepsilon_n, \quad -i\varepsilon_n. \quad (41)$$

The system is necessarily non-Hermitian because the eigenenergies are complex except for zero-energy states.

A. Zero-energy parafermion states

It follows from Eq.(41) that only the zero-energy states form a set of degenerate states respecting \mathbb{Z}_4 clock symmetry. They are \mathbb{Z}_4 parafermion states. We denote them as $|\psi_0\rangle$, $|\psi_1\rangle$, $|\psi_2\rangle$ and $|\psi_3\rangle$. They are characterized by the properties

$$\tau|\psi_0\rangle = |\psi_1\rangle, \quad \tau|\psi_1\rangle = |\psi_2\rangle, \quad (42)$$

$$\tau|\psi_2\rangle = |\psi_3\rangle, \quad \tau|\psi_3\rangle = |\psi_0\rangle, \quad (43)$$

$$\sigma|\psi_0\rangle = |\psi_0\rangle, \quad \sigma|\psi_1\rangle = i|\psi_1\rangle, \quad (44)$$

$$\sigma|\psi_2\rangle = -|\psi_2\rangle, \quad \sigma|\psi_3\rangle = -i|\psi_3\rangle, \quad (45)$$

from which the matrix representations (3) and (4) follow. Then, the \mathbb{Z}_4 parafermion relations (5) are verified. Namely, it is necessary and sufficient to examine Eqs.(7) and (8) for a triplet set of zero-energy states in order to show that they are \mathbb{Z}_4 parafermions.

B. Breathing square lattice

The quadrupole insulator has been proposed on the breathing square lattice³⁴. We propose a model possessing \mathbb{Z}_4 parafermions on the breathing square lattice. The bulk Hamiltonian is given by

$$H = \begin{pmatrix} 0 & f_x^* & 0 & if_y^* \\ -f_x & 0 & if_y^* & 0 \\ 0 & -if_y & 0 & -f_x \\ -if_y & 0 & f_x^* & 0 \end{pmatrix}, \quad (46)$$

with

$$f_x = t_a + t_b e^{ik_x}, \quad f_y = t_a + t_b e^{ik_y}, \quad (47)$$

where we have introduced two hopping parameters t_a and t_b , which are shown in Fig.1(b4).

The Hamiltonian (46) has \mathbb{Z}_4 clock symmetry²³,

$$\tau H(\mathbf{k}) \tau^\dagger = -iH(R\mathbf{k}), \quad (48)$$

where R rotates the momentum by 90 degrees as

$$R(k_x, 0) = (0, -k_y), \quad (49)$$

$$R(0, k_y) = (k_x, 0), \quad (50)$$

making the energy spectrum have \mathbb{Z}_4 symmetry in the complex plane as in Eq.(41).

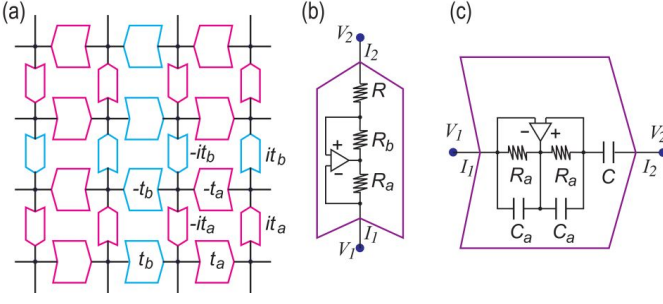


FIG. 9: (a) Electric circuit implementation of the breathing square model shown in Fig.1(b), where the hopping parameters correspond to those in Fig.1(b4). (b) Configuration of negative impedance converter with current inversion realizing imaginary hopping⁶², and (c) the one realizing nonreciprocal hopping⁶⁴, corresponding to those in (a).

C. Edge and corner states

The topological number is defined by (21), where ψ_0 is the eigen function of the Hamiltonian (46) for the bulk. We find the topological insulator phase for $|t_a/t_b| < 1$, where $Q = 1$ and the trivial insulator phase for $|t_a/t_b| > 1$, where $Q = 0$.

We calculate the energy spectrum in square geometry numerically. C_{4v} symmetry is manifest as shown in Fig.8(a). It is because the square lattice respects \mathbb{Z}_4 clock symmetry. We also show the energy spectrum as a function of t_a/t_b in Fig.8(b), where the emergence of the zero-energy states is manifest in the topological phase.

Consequently, the present model is a second-order topological insulator in the region $|t_a/t_b| < 1$, being characterized by the emergence of topological corner states.

It is possible to obtain numerically the wave functions of the four corner states. We have confirmed that they satisfy the relations (7) and (8). Therefore, they are \mathbb{Z}_4 parafermions.

D. Electric-circuit implementation

In the Hamiltonian (46), there are nonreciprocal hopping terms along the x axis. Nonreciprocal hopping is constructed by a combination of operational amplifier and capacitors⁶⁴,

$$\begin{pmatrix} I_{ij} \\ I_{ji} \end{pmatrix} = i\omega C \begin{pmatrix} -1 & 1 \\ -1 & 1 \end{pmatrix} \begin{pmatrix} V_i \\ V_j \end{pmatrix}, \quad (51)$$

It corresponds to the Hamiltonian

$$H = C \begin{pmatrix} -1 & 1 \\ -1 & 1 \end{pmatrix}. \quad (52)$$

We add an inductor or a capacitor in order to cancel the diagonal term.

We construct an electric circuit as shown in Fig.9(a), where the x axis is constructed by Fig.9(c) and the y axis is constructed by Fig.9(b).

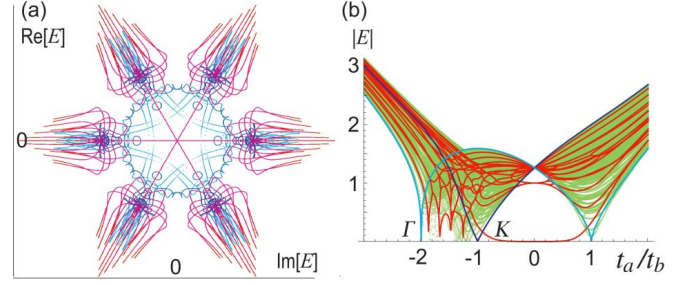


FIG. 10: Energy spectrum of a hexagon shown in Fig.1(c2). (a) the vertical axis is $\text{Re}[E]$ and the horizontal axis is $\text{Im}[E]$, while (b) the vertical axis is $|E|$ and the horizontal axis is t_a/t_b . Color indicates the value of t_a/t_b in (a). C_{6v} symmetry in the complex energy plane is manifest in (a). The emergence of zero-energy corner states is clear in (b). The green curves are calculated from the bulk Hamiltonian, while red curves are calculated based on the hexagon. The cyan curve is the energy at the Γ point, while the blue curve is the energy at the K point calculated based on the bulk Hamiltonian.

V. \mathbb{Z}_6 PARA Fermion

Finally, we construct a \mathbb{Z}_6 parafermion model. The parafermion operators are represented by the shift operator^{23,24,51}

$$\gamma_1 \equiv \tau = \begin{pmatrix} 0 & 0 & 0 & 0 & 0 & 1 \\ 1 & 0 & 0 & 0 & 0 & 0 \\ 0 & 1 & 0 & 0 & 0 & 0 \\ 0 & 0 & 1 & 0 & 0 & 0 \\ 0 & 0 & 0 & 1 & 0 & 0 \\ 0 & 0 & 0 & 0 & 1 & 0 \end{pmatrix}, \quad (53)$$

and the clock operator^{23,24,51}

$$\gamma_2 \equiv \sigma = \text{diag.} (1, \omega, \omega^2, \omega^3, \omega^4, \omega^5). \quad (54)$$

Here, τ and σ satisfy the \mathbb{Z}_6 parafermion relations,

$$\tau^6 = \sigma^6 = 1, \quad \tau\sigma = \omega\sigma\tau. \quad (55)$$

In the \mathbb{Z}_6 clock-symmetric model, the energy spectrum is composed of sextets $E_n^{(0,1,2,3,4,5)}$, $n = 0, 1, 2, \dots$,

$$E_n^{(0,1,2,3,4,5)} = \varepsilon_n, \quad \omega\varepsilon_n, \quad \omega^2\varepsilon_n, \quad \omega^3\varepsilon_n, \quad \omega^4\varepsilon_n, \quad \omega^5\varepsilon_n. \quad (56)$$

The system is necessarily non-Hermitian because the eigen energies are complex except for zero-energy states.

A Hermitian second-order topological insulator has been proposed on the breathing honeycomb lattice⁶⁵. We generalize it to a non-Hermitian model with \mathbb{Z}_6 clock symmetry by introducing complex hoppings. The bulk Hamiltonian is defined on the breathing honeycomb lattice and given by

$$H = \begin{pmatrix} 0 & \omega^2 t_b & 0 & t_a e^{ik_y} & 0 & \omega^4 t_b \\ \omega^5 t_b & 0 & \omega^3 t_b & 0 & \omega t_a e^{i\frac{-\sqrt{3}k_x + k_y}{2}} & 0 \\ 0 & t_b & 0 & \omega^4 t_b & 0 & \omega^2 t_a e^{-i\frac{\sqrt{3}k_x + k_y}{2}} \\ \omega^3 t_a e^{-ik_y} & 0 & \omega t_b & 0 & \omega^5 t_b & 0 \\ 0 & \omega^4 t_a e^{i\frac{\sqrt{3}k_x - k_y}{2}} & 0 & \omega^2 t_b & 0 & t_b \\ \omega t_b & 0 & \omega^5 t_a e^{i\frac{\sqrt{3}k_x + k_y}{2}} & 0 & \omega^3 t_b & 0 \end{pmatrix}. \quad (57)$$

We diagonalize this Hamiltonian for a hexagon shown in Fig.1(c2). C_{6v} symmetry is manifest in the complex energy plane as in Fig.10(a). Furthermore, we find six zero-energy topological corner states for $|t_a/t_b| < 1$, as shown in Fig.10(b). We also find the trivial insulator phase for $t_a/t_b < -2$ and $t_a/t_b > 1$. Additionally, there is metallic phase for $-2 < t_a/t_b < -1$.

VI. CONCLUSION

We have constructed a \mathbb{Z}_3 parafermion model on the breathing Kagome lattice, a \mathbb{Z}_4 parafermion model on the breathing

square lattice and a \mathbb{Z}_6 parafermion model on the breathing honeycomb lattice. These model exhaust all the possible realization of \mathbb{Z}_d parafermions since there are only three-fold, four-fold and six-fold rotational symmetries that are compatible with the periodic lattices. We note that two-fold symmetry corresponds to Majorana fermions.

The author is very much grateful to Y. Tanaka and N. Nagaosa for helpful discussions on the subject. This work is supported by the Grants-in-Aid for Scientific Research from MEXT KAKENHI (Grants No. JP17K05490 and No. JP18H03676). This work is also supported by CREST, JST (JPMJCR16F1 and JPMJCR20T2).

-
- ¹ G. Moore and N. Read, Nucl. Phys. B **360**, 362 (1991).
 - ² S. Das Sarma, M. Freedman, and C. Nayak, Phys. Rev. Lett. **94**, 166802 (2005).
 - ³ A. Kitaev, Annals of Physics **321**, 2 (2006).
 - ⁴ C. Nayak, S. H. Simon, A. Stern, M. Freedman, and S. Das Sarma, Rev. Mod. Phys. **80**, 1083 (2008).
 - ⁵ A. Stern, Ann. Physics **323**, 204 (2008).
 - ⁶ A. Stern, Nature **464**, 187 (2010).
 - ⁷ S. Das Sarma, M. Freedman, C. Nayak, npj Quantum Information **1**, 15001 (2015).
 - ⁸ C. W.J. Beenakker, Annu. Rev. Condens. Matter Phys. **4**, 113 (2013).
 - ⁹ T. D. Stanescu and S. Tewari, J. Phys. Condens. Matter **25**, 233201 (2013).
 - ¹⁰ S.R. Elliott and M. Franz, Rev. Mod. Phys. **87**, 137 (2015).
 - ¹¹ D. Aasen, M. Hell, R. V. Mishmash, A. Higginbotham, J. Danon, M. Leijnse, T. S. Jespersen, J. A. Folk, C. M. Marcus, K. Flensberg, and J. Alicea, Phys. Rev. X **6**, 031016 (2016).
 - ¹² D. A. Ivanov Phys. Rev. Lett. **86**, 268, (2001).
 - ¹³ B. I. Halperin, Y. Oreg, A. Stern, G. Refael, J. Alicea and F. von Oppen, Phys. Rev. B **85**, 144501 (2012).
 - ¹⁴ J. Alicea, Y. Oreg, G. Refael, F. von Oppen and M.P.A. Fisher, Nat. Phys. **7**, 412 (2011).
 - ¹⁵ X.-L. Qi, S.-C. Zhang, Rev. Mod. Phys. **83**, 1057 (2011).
 - ¹⁶ M. Leijnse and K. Flensberg, Semicond. Sci. Technol. **27**, 124003 (2012).
 - ¹⁷ J. Alicea, Rep. Prog. Phys. **75**, 076501 (2012).
 - ¹⁸ M. Sato and Y. Ando, Rep. Prog. Phys. **80**, 076501 (2017).
 - ¹⁹ Y. Tanaka, M. Sato and N. Nagaosa, J. Phys. Soc. Jpn. **81**, 011013 (2012).
 - ²⁰ Y. Kasahara, T. Ohnishi, Y. Mizukami, O. Tanaka, Sixiao Ma, K. Sugii, N. Kurita, H. Tanaka, J. Nasu, Y. Motome, T. Shibauchi, Y. Matsuda, Nature **559**, 227 (2018).
 - ²¹ A. Ahlbrecht, L. S. Georgiev, R. F. Werner, Phys. Rev. A **79**, 032311 (2009).
 - ²² P. Fendley, J. Stat. Mech. 2012, 11020 (2012).
 - ²³ P. Fendley, J. Phys. A **47**, 075001 (2014).
 - ²⁴ J. Alicea, P. Fendley, Annual Review of Condensed Matter Physics **7**, 119 (2016).
 - ²⁵ Adam S. Jermyn, Roger S. K. Mong, Jason Alicea, and Paul Fendley, Phys. Rev. B **90**, 165106 (2014).
 - ²⁶ H. Ebisu, E. Sagi, Y. Tanaka, and Y. Oreg, Phys. Rev. B **95**, 075111 (2017).
 - ²⁷ A. Hutter and D. Loss, Phys. Rev. B **93**, 125105 (2016).
 - ²⁸ R. J. Baxter, Phys. Lett. A **140**, 155 (1989); J. Statist. Phys. **57**, 1 (1989).
 - ²⁹ N. Read and E. Rezayi, Phys. Rev. B **59**, 8084 (1999).
 - ³⁰ D. J. Clarke, J. Alicea, K. Shtengel, Nat. Com. **4**, 1348 (2013).
 - ³¹ K. Laubscher, D. Loss, J. Klinovaja, Phys. Rev. Research **1**, 032017 (2019).
 - ³² K. Laubscher, D. Loss, J. Klinovaja, Phys. Rev. Research **2**, 013330 (2020).
 - ³³ F. Zhang, C.L. Kane and E.J. Mele, Phys. Rev. Lett. **110**, 046404 (2013).
 - ³⁴ W. A. Benalcazar, B. A. Bernevig, and T. L. Hughes, Science **357**, 61 (2017).
 - ³⁵ F. Schindler, A. Cook, M. G. Vergniory, and T. Neupert, in APS March Meeting (2017).
 - ³⁶ Y. Peng, Y. Bao, and F. von Oppen, Phys. Rev. B **95**, 235143 (2017).
 - ³⁷ J. Langbehn, Y. Peng, L. Trifunovic, F. von Oppen, and P. W. Brouwer, Phys. Rev. Lett. **119**, 246401 (2017).
 - ³⁸ Z. Song, Z. Fang, and C. Fang, Phys. Rev. Lett. **119**, 246402 (2017).

- ³⁹ W. A. Benalcazar, B. A. Bernevig, and T. L. Hughes, *Phys. Rev. B* **96**, 245115 (2017).
- ⁴⁰ F. Schindler, A. M. Cook, M. G. Vergniory, Z. Wang, S. S. P. Parkin, B. A. Bernevig, and T. Neupert, *Science Advances* **1**, eaat0346 (2018).
- ⁴¹ C. Fang, L. Fu, *Science Advances* **5**, eaat2374 (2019).
- ⁴² M. Ezawa, *Phys. Rev. Lett.* **120**, 026801 (2018).
- ⁴³ M. Ezawa, *Phys. Rev. B* **98**, 045125 (2018).
- ⁴⁴ M. Geier, L. Trifunovic, M. Hoskam, and P. W. Brouwer, *Phys. Rev. B* **97**, 205135 (2018).
- ⁴⁵ E. Khalaf, *Phys. Rev. B* **97**, 205136 (2018).
- ⁴⁶ M. Ezawa, *Phys. Rev. B* **100**, 045407 (2019).
- ⁴⁷ T. Liu, Y.-R. Zhang, Q. Ai, Z. Gong, K. Kawabata, M. Ueda, F. Nori, *Phys. Rev. Lett.* **122**, 076801 (2019).
- ⁴⁸ M. Ezawa, *Phys. Rev. B* **99**, 201411(R) (2019).
- ⁴⁹ M. Ezawa, *Phys. Rev. B* **99**, 121411(R) (2019).
- ⁵⁰ E. Edvardsson, F. K. Kunst, E. J. Bergholtz, *Phys. Rev. B* **99**, 081302 (2019).
- ⁵¹ G. Ortiz, E. Cobanera, Z. Nussinov, *Nuc. Phys. B* **854**, 780 (2012).
- ⁵² X. Ni, M. Weiner, A. Alu and A. B. Khanikaev, *Nature Materials* **18**, 113 (2019).
- ⁵³ Z. Gong, Y. Ashida, K. Kawabata, K. Takasan, S. Higashikawa and M. Ueda, *Phys. Rev. X* **8**, 031079 (2018).
- ⁵⁴ K. Kawabata, K. Shiozaki, M. Ueda, and M. Sato, *Phys. Rev. X* **9**, 041015 (2019).
- ⁵⁵ S. Imhof, C. Berger, F. Bayer, J. Brehm, L. Molenkamp, T. Kiessling, F. Schindler, C. H. Lee, M. Greiter, T. Neupert, R. Thomale, *Nat. Phys.* **14**, 925 (2018).
- ⁵⁶ C. H. Lee, S. Imhof, C. Berger, F. Bayer, J. Brehm, L. W. Molenkamp, T. Kiessling and R. Thomale, *Communications Physics*, **1**, 39 (2018).
- ⁵⁷ T. Helbig, T. Hofmann, C. H. Lee, R. Thomale, S. Imhof, L. W. Molenkamp and T. Kiessling, *Phys. Rev. B* **99**, 161114 (2019).
- ⁵⁸ Y. Lu, N. Jia, L. Su, C. Owens, G. Juzeliunas, D. I. Schuster and J. Simon, *Phys. Rev. B* **99**, 020302 (2019).
- ⁵⁹ Y. Li, Y. Sun, W. Zhu, Z. Guo, J. Jiang, T. Kariyado, H. Chen and X. Hu, *Nat. Com.* **9**, 4598 (2018).
- ⁶⁰ M. Ezawa, *Phys. Rev. B* **98**, 201402(R) (2018).
- ⁶¹ M. Serra-Garcia, R. Susstrunk and S. D. Huber, *Phys. Rev. B* **99**, 020304 (2019).
- ⁶² T. Hofmann, T. Helbig, C. H. Lee, M. Greiter, R. Thomale, *Phys. Rev. Lett.* **122**, 247702 (2019).
- ⁶³ M. Ezawa, *Phys. Rev. B* **102**, 075424 (2020).
- ⁶⁴ T. Helbig, T. Hofmann, S. Imhof, M. Abdelghany, T. Kiessling, L. W. Molenkamp, C. H. Lee, A. Szameit, M. Greiter, R. Thomale, *Nature Physics* **16**, 747 (2020).
- ⁶⁵ T. Mizoguchi, H. Araki and Y. Hatsugai, *J. Phys. Soc. Jpn.* **88**, 104703 (2019).